JVSTB Journal of Vacuum Science & Technology B

Monte Carlo simulation of process parameters in electron beam lithography for thick resist patterning

Jianyun Zhou and XiaoMin Yang

Citation: Journal of Vacuum Science & Technology B **24**, 1202 (2006); doi: 10.1116/1.2192543
View online: http://dx.doi.org/10.1116/1.2192543
View Table of Contents: http://scitation.aip.org/content/avs/journal/jvstb/24/3?ver=pdfcov
Published by the AVS: Science & Technology of Materials, Interfaces, and Processing

Monte Carlo simulation of process parameters in electron beam lithography for thick resist patterning

Jianyun Zhou and XiaoMin Yang[a)]
Seagate Research Center, 1251 Waterfront Place, Pittsburgh, Pennsylvania 15222

(Received 27 December 2005; accepted 9 March 2006; published 24 April 2006)

To better understand the proximity effect of electron-beam lithography and its limitation on aspect ratios in a thick resist film (>1.0 μm), the simulation of isolated trench patterning has been performed using the Monte Carlo simulation software SELID™. Various key process parameters, including beam energy, exposure dose, substrate, acid diffusion length, and development time have been analyzed by means of the point-spread function, secondary electron distribution, energy distributions, and developed resist profiles. Exposure dose and development time are optimized to achieve vertical sidewalls, and the acid diffusion length has been adjusted to slightly change the top and bottom dimensions of the patterned trench. The simulation results show that increasing the beam energy significantly reduces the forward proximity effect and thereby increases the trench aspect ratio. In contrast, the substrate generally has only a minor effect in terms of the resist profile because its backscattering effect covers a long range up to 10.0 μm from incident point (50 keV). The achievable maximum aspect ratio for a given resist thickness was found to scale approximately linearly with beam energy. The aspect ratio in a 1.0 μm thick resist film increased from 3:1 to 20:1 as the beam energy was increased from 10 to 100 keV, and from 5:1 to 10:1 for a 4.0 μm resist film as the beam energy was increased from 50 to 100 keV. Finally, experimental data using a 50 keV Leica e-beam writing tool is presented, and they agree with the results from our simulations. [DOI: 10.1116/1.2192543]

I. INTRODUCTION

The merits of electron beam lithography are widely recognized as providing better resolution and greater accuracy compared with optical lithography. Because of these advantages, electron beam lithography has been used for many years in photomask patterning, direct writing on semiconductor devices, and research for the fabrication of various nanodevices. Although electron beam lithography can provide a focused electron beam at dimensions of less than 10 nm, several factors besides the size of the electron beam determine the extent of the exposed volume in the resist and, consequently, the developed spatial contour or profile in the resist. One of the major factors is the proximity effect due to electron scattering in the resist and substrate. Simulations have proven to be an effective way of understanding the proximity effect, and thereby improve the electron beam lithography process.

The most critical issue in the e-beam simulation work is to understand the interaction between the electrons and the resist. Several different models to describe this interaction have been developed previously and include the point incidence method,[1] Gaussian fit models (double Gaussian and triple Gaussian),[2,3] and the Monte Carlo model.[4] The point incidence model calculates energy deposition by arranging electron incidence points over the exposure area and summing up proximity effects from each incidence point. It is analogous to the real exposure system and gives accurate results, but has the drawback of extremely long computation time. Gaussian fit models normally use one Gaussian term to account for small-range forward scattering and one or more Gaussian terms to represent backscattering to give an overall energy deposition distribution function. While the double Gaussian model has issues with complicated underlayers and high-resolution features, triple- and multi-Gaussian models seem to address these problems. A drawback with the Gaussian fit models, however, is that the parameter values, in the Gaussian terms, need to be carefully determined by either Monte Carlo techniques or experimental measurements. Recently, Rooks *et al.* have presented the optimization of forward scattering parameter by an efficient experimental technique.[5] Monte Carlo models, which are most commonly used in modeling work today, simulate the multiple scattering acts of electrons in resist based on the Rutherford scattering cross-section model and calculate energy deposition using Bethe's continuous energy loss approximation. The model then takes the statistical average of the deposited energy of all simulated electrons to give a point-spread function (PSF), also called proximity function, whose accuracy depends on the number of electrons used. The number of electrons used in the simulation may be adjusted to provide for increased accuracy at the expense of increased computation time.

In this article, we will present the results from the Monte Carlo simulation of high aspect ratio isolated trench patterning in thick resist. The resist thicknesses used ranged from 1.0 to 4.0 μm and were chosen on the basis of their application in the magnetic data storage industry. Small critical dimensions (CD) with aspect ratios of 7:1–10:1 are generally

[a)]Author to whom correspondence should be addressed; electronic mail: xiaomin.yang@seagate.com

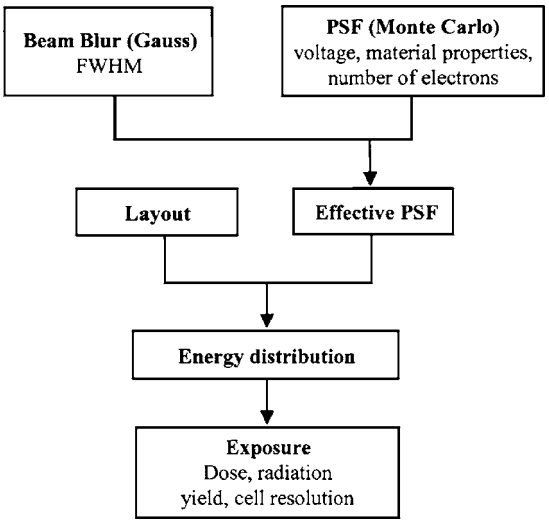

FIG. 1. Block diagram of steps of SELID exposure simulation.

required to fabricate the critical magnetic structures such as the write top pole in thin film head devices.[6–10] In this work, the physical mechanism and impact of the proximity effect are studied in depth as they relate to the resist sidewall profiles and CD control. To achieve vertical sidewalls, many factors have been investigated here including different substrate materials, resist thicknesses, exposure doses, acid diffusion lengths, and development times. Experimental data obtained using a direct-write e-beam tool are also presented for comparison with the simulation results.

II. SIMULATION AND EXPERIMENTAL DETAILS

A. Simulation model and structure

SELID™ software, developed by Sigma-C, has been used in our simulation work. SELID™ uses the Monte Carlo model to optimize the trade-off between accuracy and computation time for different application requirements. SELID™ is a shaped beam electron-beam lithography (EBL) simulator, yet its use in Gaussian beam systems has been verified to be accurate.[11] The simulation flow is shown in Fig. 1. First, the Monte Carlo PSF is calculated using Rutherford's cross-section model for elastic scattering, Bethe's continuous slowing down model for inelastic scattering, and Moller's cross-section model for fast secondary electron generation. The Monte Carlo PSF is then combined with a beam blur to generate an effective point spread function, which in turn interacts with the layout to determine energy distribution in the resist. The energy distribution, dose, and radiation yield are used as input parameters for the development simulation during which local resist dissolution rates are calculated and combined with development time and cell resolution to give a final resist profile.

The most time consuming step in the SELID™ simulation is the Monte Carlo PSF calculation. The SELID™ software has the capability of saving all calculated Monte Carlo PSFs in a library. Computation time is greatly reduced by the software's ability to match an exposure condition with the corresponding PSF saved within the library.

B. Simulation conditions

In the simulations, we have specified a 3.0 μm thick film of generic positive tone chemically amplified resist (CAR) as the resist, bulk silicon as substrate, and a CAD design of 250 nm isolated lines as our layout feature unless otherwise specified. The diffusion length, which is determined by resist type and postexposure bake conditions, was chosen to be 40 nm. This is a common diffusion length for CARs as indicated in other works.[12,13] The development process is simulated using Mack's four-parameter development model[14] having parameters $R_{max}=0.225$ μm/s, $R_{min}=0.000\,01$ μm/s, $M_{th}=0.26$, and $N=6.85$. In Mack's model, R_{max} is the development rate of a completely exposed resist, R_{min} is the development rate of totally unexposed resist, M_{th} is the threshold inhibitor concentration relative to the inhibitor concentration constant, and N is the selectivity parameter that describes the sensitivity of the developer to the exposed resist. The coordinate system is chosen such that the x-y plane is parallel to the resist surface, where $z=0$ is the substrate surface, and $z+$ is pointing from the substrate surface into the resist.

C. Experiment conditions

For the experimental work, the ebeam exposure was performed using a Leica VB6 direct-write vector beam lithography system operating at 50 keV with an 800 μm field size and 12.5 nm grid size. The chemically amplified resists used in this work was TOK EP-GM005 (OHKA, Inc.). The resist was prebaked at 130 °C for 90 s. before exposure and the postexposure bake (PEB) was 110 °C for 90 s. Development was performed on a FSI 2000 cluster tool using NMD-3 TOK TMAH (tetramethylammonium hydroxide) developer for 60 s. All cross-section images were taken using a Hitachi scanning electron microscopy (SEM).

III. RESULTS AND DISCUSSION

For e-beam process of positive CARs, incident electrons interact with the resist atoms through collisions during exposure, and low energy (<50 eV) secondary electrons are generated along the path of the primary electrons. These secondary electrons will slow down gradually thus transfer their energy into the resist. Acid is generated during PEB process, which will diffuse and catalyze in the exposed areas. These exposed areas then dissolve in the developer during development and the final resist profile is determined. Many parameters contribute to this process, among which are the e-beam source energy, substrate material, and exposure dose which all relate to the exposure process, whereas acid diffusion and development time relate to the PEB and development conditions, respectively. All of the above parameters contribute to the proximity effect, thus will affect the final resist profile. Our simulations have shown that beam energy, substrate ma-

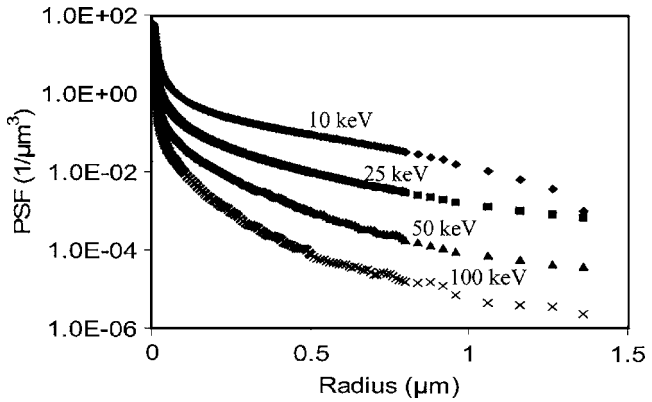

FIG. 2. Averaged point spread function of electron beams incident on 3.0 μm generic CAR with silicon substrate.

terial, exposure dose, acid diffusion length, and development time are the most important parameters. Their effects are analyzed and discussed in detail below.

A. Beam energy effect

The effect of beam energy on the resist profile has been examined by using PSF, secondary electron distribution, and energy distributions for beam energies ranging from 10 to 100 keV. The PSF is a three-dimensional probability density function generated by the Monte Carlo simulation that represents the distribution of the accumulated energy of one single electron in the resist. PSF is strongly dependent on beam energy. An example of a one-dimensional averaged PSF as a function of beam energy is displayed in Fig. 2. The average of PSF is taken in the z direction throughout the resist film thickness. The data show that the probability of energy deposition in the resist is lower for higher energy beams. We roughly estimated that in the 0.3–1.0 μm range, the PSF is reduced to approximately 1/10th of its original value when the beam energy is doubled. This is because the energy loss of the electrons per unit path length and the scattering cross section decrease with increasing beam energy,[15] which indicates a better throughput of low energy electrons.

Secondary electrons generally have low energy and their mean free path is around 1 nm. Consequently their distribution is highly dependent on the trajectory of primary electrons and is representative of electron's scattering behavior. Figure 3 shows the secondary electron distribution in full range (a) and within resist (b) for beam energy ranging from 10 to 100 keV. 5000 primary electrons are used for 10–50 keV, and 10 000 for 100 keV. The width and depth of secondary electron distribution, representing the lateral spread and penetration depth of primary electrons, respectively, have increased with beam energy, and in particular, the penetration depth increases proportional to the acceleration voltage (V) as $V^{3/2}$.[16] However, within resist film, as seen in Fig. 3(b), the lateral spread is larger for low energy beams, and lower for high energy beams. The larger relative lateral spread for a low energy beam is explained by the fact that the low energy beam is more easily deflected and spreads out along the lateral direction. For a 10 keV electron beam, the secondary electron distribution shows that the penetration depth is about 1.5 μm, thus it could not penetrate the 3.0 μm thick resist. In addition, low energy beam has shown

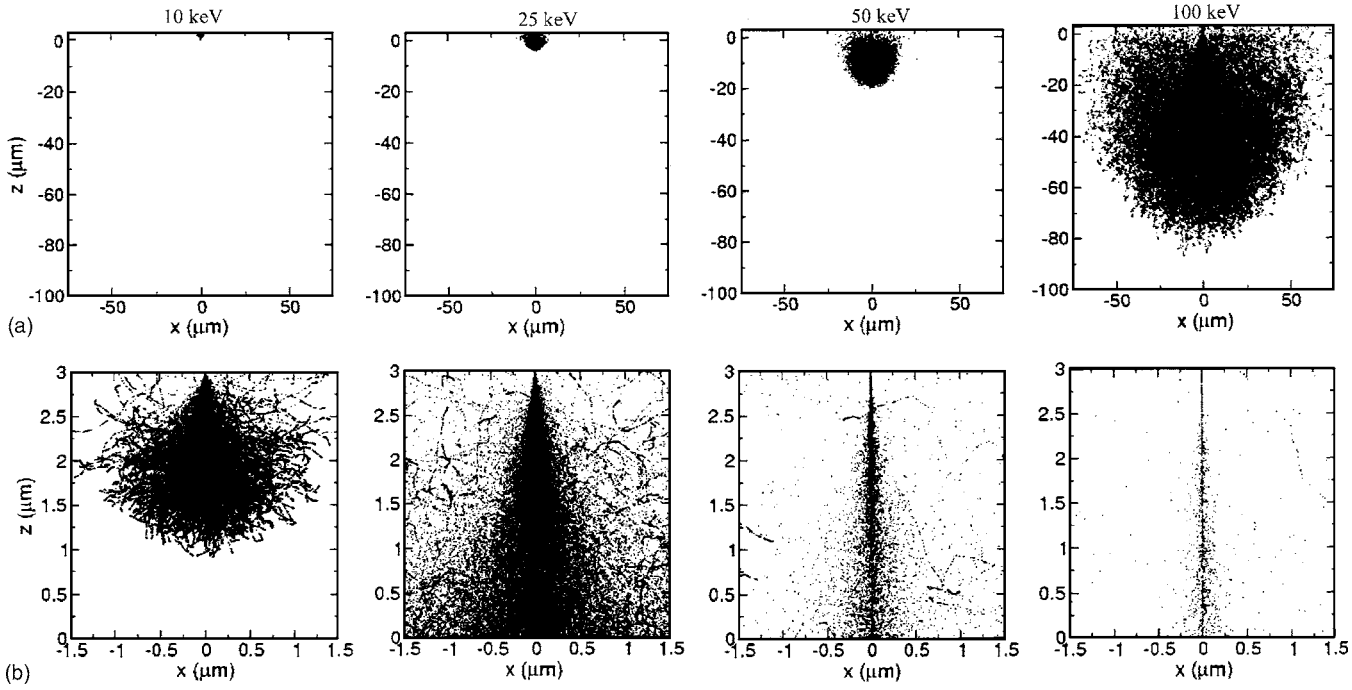

FIG. 3. Secondary electron distribution (a) in resist and substrate (b) within resist as a function of beam energy. Corresponding primary electrons are 5000 for 10–50 keV and 10 000 for 100 keV.

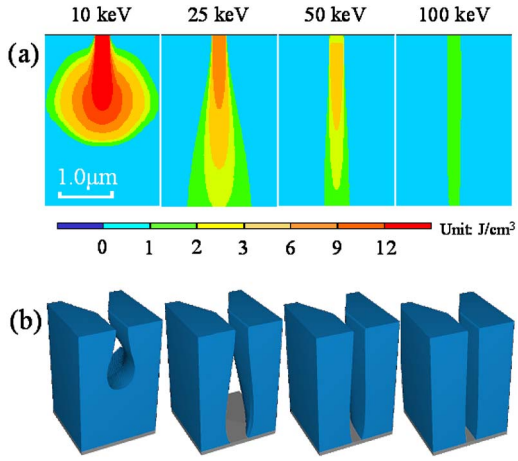

FIG. 4. (a) Two-dimensional (2D) energy density distribution in a 3.0 μm generic CAR on silicon substrate as a function of beam energy. Corresponding exposure dose is 5.0 μC/cm^2. (b) Developed top-pole structure profiles in 3.0 μm generic CAR exposed at 10, 25, 50, and 100 keV.

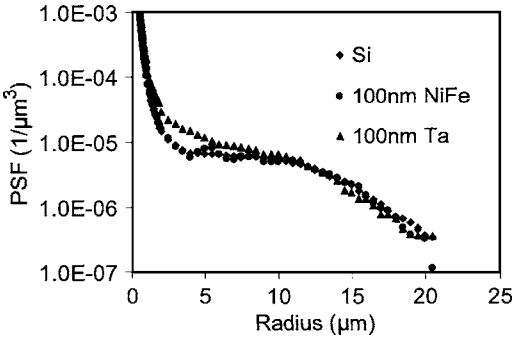

FIG. 5. Averaged point spread function of 50 keV electron beam incident on 3.0 μm generic CAR with different substrate materials.

much higher secondary electron density, indicating more energy deposition, consistent with the previous conclusion of better throughput for low energy beams.

The scattering of electrons has practical consequences, especially for the thick resist process. As electrons go through the resist, the small angle scattering effect accumulates and results in a broadened energy distribution at the resist-substrate interface as compared to the resist top. Figure 4(a) shows energy density contours corresponding to different beam energies. The dose used for all beam energies are 5 μC/cm^3. The total energy deposition in the resist has decreased with increase of beam energy, consistent with the theory that energy loss of the electrons per unit path length and the scattering cross section decreases with beam energy. The energy contours has shown similar pattern as secondary electron density in Fig. 3, with broadening at resist bottom, and this broadening worsens as beam energy is reduced. Figure 4(b) shows the simulated patterning results of top pole structure of thin film head[8] as a function of beam energy. The nominal pole width is 250 nm. These resist profiles very closely follow the energy contours as shown in Fig. 4(a), assuming that the threshold energy contour is chosen. A low energy beam of 10 keV will only penetrate to half the depth of a 3.0 μm thick resist film, resulting in a half-open trench with the bottom CD wider than the top CD by a factor of ~2. A 25 keV beam also produces a trench with a bottom CD to top CD ratio of 2, but with the resist trench open to the substrate. In contrast, higher energy beams give relatively straight sidewalls. A 50 keV beam broadened the nominal CD by ~40% at the resist bottom, whereas a 100 keV beam broadened the nominal CD by only ~10%. This implies that in a 3.0 μm thick resist film, a beam energy of 100 keV is required in order to achieve vertical sidewalls. This conclusion can be generalized to other resist thicknesses, with corresponding beam energy requirements.

B. Substrate effect

The substrate and underlying metallic layers, such as the seed layer for electroplating, certainly affect the e-beam processes due to their backscattering effect. This is especially true for high-Z materials. High-Z materials give a higher probability of large angle scattering of electrons due to their relatively larger nucleus. Increasing the high-Z material film thickness is also expected to increase the backscattering intensity. Simulations have been conducted using bare silicon substrates, and silicon substrates coated with NiFe, and Ta layers. In order to understand the difference of backscattering in the different under layer materials, we calculated the PSFs, shown in Fig. 5. The PSF graph shows that within 0.5 μm from the incident point, there is no significant difference between the different under layers. This is primarily due to the fact that within this range forward scattering dominates and backscattering is negligible. In the range of 0.5–10.0 μm, backscattering becomes dominant and there is higher energy deposition for high-Z underlayers. Beyond 10.0 μm from the incidence point, no significant difference is observed in PSF. This is in agreement with other work's conclusion that the backscattering range for 50 keV beam is 10.0 μm.

We do not expect much difference in the developed resist profile between the various substrates because each shows evidence of long-range backscattering effects (as seen from their PSF) but here we are only concerned with the isolated small feature areas. The simulation results, in Fig. 6, are generally consistent with our expectations. The sole exception was in the 25 keV case, which has obviously broadened at the bottom of the resist where the 100 nm Ta layer was added. From a trajectories comparison for 25 keV in Fig. 7, the penetration depth has decreased with the increase in the layer's atomic number Z, while the number of backscattered electrons has increased, particularly for the Ta underlayer. The backscattered electrons add exposure to the resist that already possesses close-to-threshold energy deposition from forward scattered electrons, thereby pushing the resist above the threshold to become developable. For the higher energies, 50 and 100 keV beams, a 100 nm thick underlayer is not thick enough to change the backscattering significantly, so there is no significant difference in the profiles. The quan-

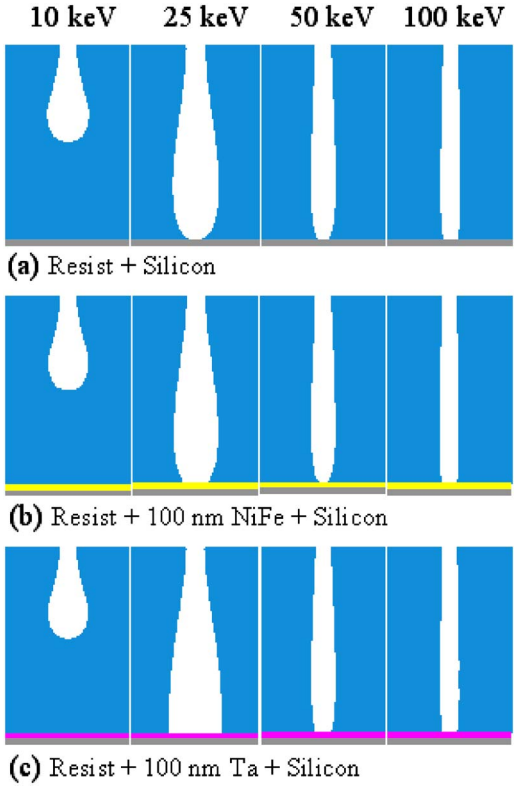

FIG. 6. 2D resist profiles of 3.0 μm generic CAR on substrate (a) silicon, (b) 100 nm NiFe layer, and (c) 100 nm Ta layer. Corresponding doses from left to right are 0.9, 5.0, 6.5, and 12.0 μC/cm^2, respectively.

tified backscattering intensity as a function of underlayer's thickness and beam energy will be researched in more detail in future work.

C. Dose/resist thickness effects

The resist profile dependence on exposure dose and resist thickness has been simulated for a 50 keV beam in a 1.0–4.0 μm thick resist film on a silicon substrate. The broadening effect at the resist bottom increases with increased resist thickness and exposure dose. As the resist thickness increases, the cumulative scattering effect also increases at the resist bottom, resulting in an increased bottom CD. As the dose is increased, the energy deposited into the resist increases and a greater percentage of the resist achieves the threshold energy to become developable. The optimal dose that gives us the best profile is the minimum dose to open the trench.

D. Acid diffusion length during PEB

For chemically amplified resists, photogenerated acid is produced and starts to diffuse during the PEB process. The diffusion results in acid redistribution, which will determine the final resist profile. The diffusion of acid is dependent on the PEB conditions as well as the resist properties. In our simulation, the PEB conditions, such as PEB temperature and time, and resist properties are integrated into one single parameter, acid diffusion length. Figure 8 shows that the bot-

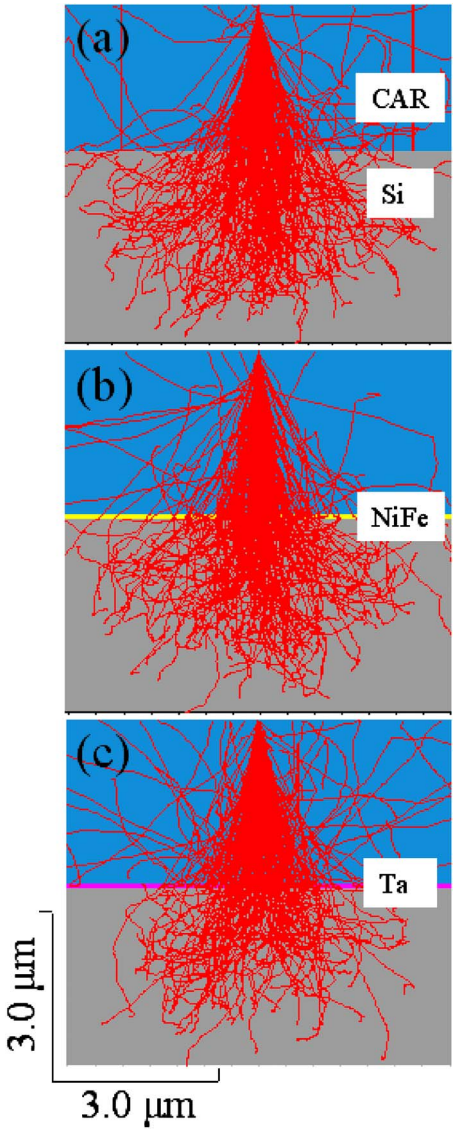

FIG. 7. Electron trajectories of 25 keV electron beam in 3.0 μm generic CAR on substrate (a) silicon, (b) 100 nm NiFe layer, and (c) 100 nm Ta layer.

tom CD decreases drastically while the top CD increases slightly with increasing acid diffusion length.

To understand this discrepancy, normalized acid concentration distributions at the top of the resist and the resist-substrate interface have been investigated (Fig. 9). It is obvious that the acid concentration distribution flattens as the acid diffusion length increases. Whether CDs will increase or decrease is determined by where the threshold acid concentration is located. For example, if the threshold concentration is 0.6 as shown in Fig. 9(a), the top CD would be represented by the line connecting points "a" and "b" with no diffusion. Note that the feature CD is roughly independent of acid concentration for a zero diffusion length. A diffusion length of 0.04 μm for the same acid threshold concentration would yield a top CD represented by the line connecting points "c" and "d," indicating a line width decrease. In contrast, if the threshold concentration is 0.2, the CD for a diffusion length

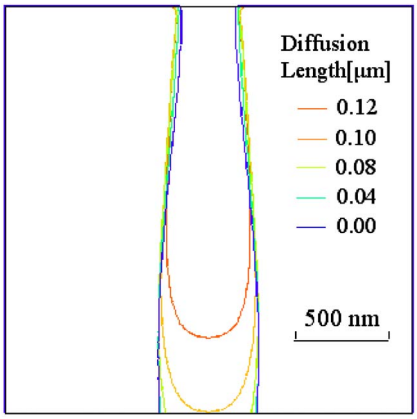

FIG. 8. 2D resist profiles of 3.0 μm generic CAR exposed with 50 keV electron beam with different diffusion lengths.

of 0.04 μm would be represented by the line connecting points "e" and "f," indicating a top CD increase. Due to the fact that the acid distribution is a normalized concentration instead of an absolute value, and the top energy deposition and acid concentration is larger than that at the bottom (as seen in Fig. 4), the situation here is that the absolute value of threshold concentration lies in the normalized increasing range (0–0.4) for the resist top, and in the decreasing range (0.4–0.7) for the resist bottom, which leads to our observing increasing top CD and decreasing bottom CD.

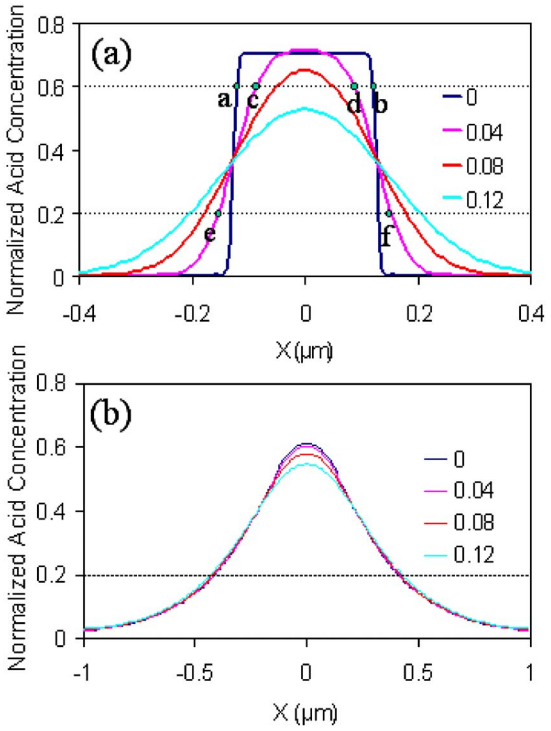

FIG. 9. Normalized acid distribution (a) at resist top (b) at resist-substrate interface of 3.0 μm generic CAR after PEB, with diffusion length of 0.0, 0.04, 0.08, and 0.12 μm, respectively.

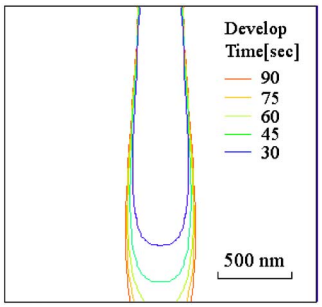

FIG. 10. 2D resist profiles of 3.0 μm generic CAR exposed with 50 keV electron beam with different development times.

E. Development time

During development process, the resist at different locations dissolves at different dissolution rates due to varying acid concentrations instead of an ideal threshold cutoff. A development front was introduced to model this process.[17] The development front is defined simply as the resist surface plane at $t=0$. At time $t>0$, the plane will propagate perpendicular to the front plane with a speed proportional to the local solubility of the resist, which is dependent on energy deposition for traditional resists and on the acid concentration for CARs. Figure 10 shows simulated resist profiles for development times of 30, 45, 60, 75, and 90 s, respectively. This figure shows that the top CD increases at the relatively low rate of less than 0.33 nm/sec, whereas the bottom CD increases at a much higher rate of about 2 nm/sec, causing a decrease in sidewall angle which is defined as the angle between substrate and resist sidewall inside the trench. The rate of increase of the bottom CD declines rapidly with development time. In addition, the CD variation of the cross section is increased because the local solubility difference is magnified with increased development time.

F. Aspect ratio limits

The aspect ratio is defined as the ratio of the resist thickness to the feature CD. Considering the broadening effect at the bottom of the features in thick resist, we define the aspect ratio as the ratio of the resist thickness to the bottom CD. For the purpose of this work, this definition is valid only when the difference between the bottom CD and top CD is less than 4% of resist thickness, or equivalently the sidewall angle $\theta>89°$. The simulation results show that the achievable aspect ratio increases with beam energy but decreases with resist thickness (Fig. 11). For a 1.0 μm thick resist film, the aspect ratio increases from about 3:1 to 20:1 when increasing the beam voltage from 10 to 100 keV. When we increase the beam voltage from 25 to 100 keV, the aspect ratios for the 2.0 and 3.0 μm thick resists have increased from 5:1 to 17:1, and 4:1 to 15:1, respectively. For a 4.0 μm thick resist film, the aspect ratio has increased from 5:1 to 10:1 when raising the beam voltage from 50 to 100 keV.

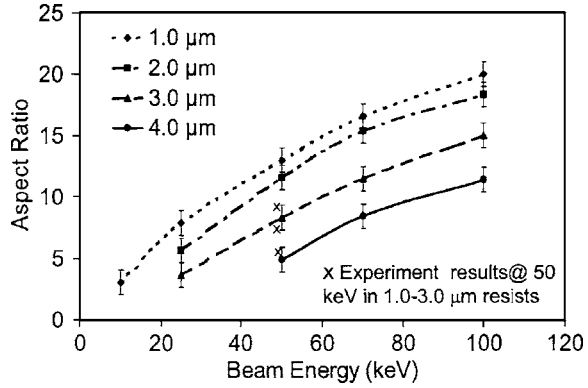

FIG. 11. Maximum aspect ratio achievable at different beam energies and resist thicknesses from simulation, with comparison to experiment aspect ratios at 50 keV in 1.0–3.0 μm resists.

G. Comparison of the simulations with the experimental results

TOK-EP-GM005 positive tone CAR with thicknesses of 1.0–4.0 μm was used in our experimental studies. The layout patterns were 100 nm isolated lines for 1.0 μm of resist, 200 nm isolated lines for 2.0 μm of resist, 300 nm isolated lines for 3.0 μm of resist, and 400 nm isolated lines for 4.0 μm of resist. All lines were spaced at 10.0 μm, with 30 lines per array. The electron beam was generated with a 50 kV acceleration voltage. Doses used were 100–135 μC/cm^2 for the 1.0 μm film, 80–115 μC/cm^2 for the 2.0 μm film, 100–135 μC/cm^2 for the 3.0 μm film, and 175–210 μC/cm^2 for the 4.0 μm film. Cross-section SEM images of the resists are shown in Fig. 12, with comparisons to simulation results. A broadened trench bottom is observed in both experimental and simulation results, and a critical dose exists where both top and bottom CDs are relatively small while maximum CD is achieved at about 2/3 depth of the resist film. Vertical sidewall is achieved in 1.0 μm resist, beyond 2.0 μm, no vertical sidewall can be achieved with 50 keV electron beam.

The aspect ratio of the different TOK resist thicknesses has been calculated from our experimental results. Comparisons with simulation results are displayed in Fig. 11. In all cases the experimental aspect ratio is lower than the simulation, and the difference between experimental and simulation aspect ratios is roughly constant. This is explained by differences in the acid diffusion length and the development selectivity between the resists used in the experiments and the simulations.

IV. CONCLUSIONS

The e-beam lithography simulation software SELID™ has been employed to investigate the proximity effect and many key process parameters in the thick resist process. Forward scattering effects are more severe than back scattering effects and limit the achievable aspect ratio by causing the bottom CD to broaden. Increasing the beam energy improves the forward proximity effect significantly, and a 100 keV beam can achieve straight sidewalls in a 3.0 μm thick resist film.

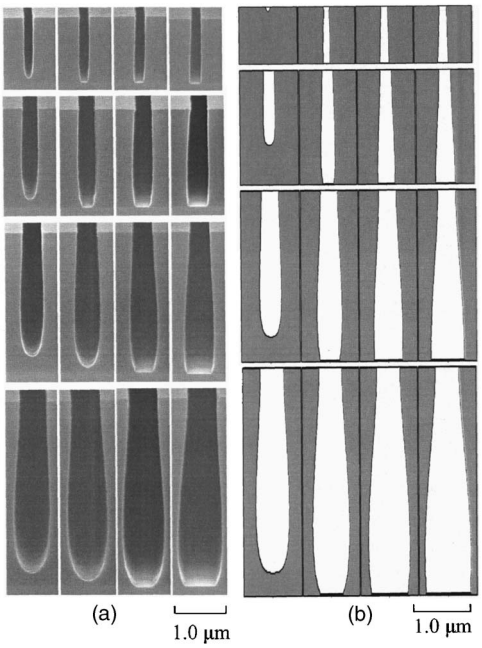

FIG. 12. Experimental resist profiles as a function of exposure dose for thicknesses ranging from 1.0 to 4.0 μm, and corresponding simulation profiles. The nominal CD is 100 nm for 1.0 μm resist, 200 nm for 2.0 μm resist, 300 nm for 3.0 μm resist, and 400 nm for 4.0 μm resist. Exposure dose is 100–130 μC/cm^3 for 1.0 μm resist, 85–115 μC/cm^3 for 2.0 μm resist, 100–130 μC/cm^3 for 3.0 μm resist, and 175–205 μC/cm^3 for 4.0 μm resist.

The substrate generally has only minor effects on the developed resist sidewall profile, although high-Z materials will increase backscattering as compared to bare silicon. Exposure dose and development time have been optimized to achieve the most vertical sidewall, while PEB conditions have been adjusted to slightly change the top and bottom CD. Simulation results have shown that the achievable aspect ratio increases with beam energy, but decreases with resist thickness. Achievable aspect ratios were found to scale approximately linearly with beam energy.

Experimental work was performed to verify the accuracy of the simulation results and shows good consistency. More experimental work is needed to search for a practical solution to the sidewall angle and CD control problem. Shrink processes could be employed to push CDs smaller, and proximity corrections may possibly address the sidewall problem.

ACKNOWLEDGMENTS

This research work is sponsored by Seagate Technology in collaboration with the Industrial Leadership in Physics Program of Georgetown University during the internship of one of the authors (J.Z.). The authors would like to thank the lithography team, especially Shuaigang Xiao for experimental assistance, Werner Scholz for data analysis, and John Lewellen and Peter Brooker from Sigma-C for their helpful discussion.

[1]A. Moniwa, H. Yamaguchi, and S. Okazaki, J. Vac. Sci. Technol. B **10**, 2771 (1992).
[2]R. Rau, J. H. McClellan, and T. J. Drabik, J. Vac. Sci. Technol. B **14**, 2445 (1996).
[3]M. Osawa, K. Takahashi, M. Sato, H. Arimoto, K. Ogino, H. Hoshino, and Y. Machida, J. Vac. Sci. Technol. B **19**, 2483 (2001).
[4]M. Gentili, L. Grella, A. Lucchesini, L. Luciani, L. Mastrogiacomo, and P. Musumeci, J. Vac. Sci. Technol. B **8**, 1867 (1990).
[5]M. Rooks, N. Belic, E. Kratschmer, and R. Viswanathan, J. Vac. Sci. Technol. B **23**, 2769 (2005).
[6]X.-M. Yang, A. Eckert, K. Mountfield, H. Gentile, C. Seiler, S. Brankovic, and E. Johns, J. Vac. Sci. Technol. B **21**, 3017 (2003).
[7]X.-M. Yang, J. Vac. Sci. Technol. B **23**, 2624 (2005).
[8]A. Eckert and K. Mountfield, J. Vac. Sci. Technol. B **22**, 2936 (2004).
[9]X.-M. Yang, H. Gentile, A. Eckert, and S. R. Brankovic, J. Vac. Sci. Technol. B **22**, 3339 (2004).
[10]M. J. Rooks, E. Kratschmer, and R. Viswanathan, J. Vac. Sci. Technol. B **20**, 2937 (2002).
[11]J. H. Tortai, J. Thiault, R. Tiron, L. Mollard, S. Haefele, S. Vychub, J. Lewellen, and P. Brooker, Proceedings of European Mask and Lithography Conference (EMLC), 2005 (unpublished).
[12]T. Itani, S. Hashimoto, M. Yamana, N. Samoto, and K. Kasama, Microelectron. Eng. **41/42**, 363 (1998).
[13]J.-B. Kim, J.-H. Choi, Y.-G. Kwon, M.-H. Jung, and K.-H. Chang, Polymer **40**, 1087 (1999).
[14]J. Thackeray, T. H. Fedynyshyn, D. Kang, and M. M. Rajaratnam, J. Vac. Sci. Technol. B **14**, 4267 (1996).
[15]L. F. Thompson, C. G. Wilson, and M. J. Bowden, *Introduction to Microlithography* (United Book Press Inc., Baltimore, MD, 1994), pp. 85–109.
[16]S. Rizvi, *Handbook of Photomask Manufacturing Technology* (Taylor & Francis, London/Boca Raton, FL, 2005), pp. 60–95.
[17]I. Raptis, N. Glezos, E. Valamontes, E. Zervas, and P. Argitis, Vacuum **62**, 263 (2001).